

***Ab initio* molecular-orbital study of the trichlorine radical, Cl₃**

A. L. Kaledin, M. C. Heaven, W. G. Lawrence, Q. Cui, J. E. Stevens,
and K. Morokuma

*Cherry L. Emerson Center for Scientific Computation and Department of Chemistry, Emory University,
Atlanta, Georgia 30322*

(Received 10 October 1997; accepted 11 November 1997)

We report a rigorous *ab initio* study of the ground and low-lying excited-state potential-energy surfaces (PESs) of the Cl₃ radical at CASSCF, CASPT2, and MRSDCI levels of theory. The ground state has two Cl⋯Cl₂ van der Waals complexes, $\tilde{\mathbf{X}}\mathbf{L}$ and $\tilde{\mathbf{X}}'\mathbf{B}$. The linear asymmetric minimum ($\tilde{\mathbf{X}}\mathbf{L}$) is ${}^2\Pi$, with a Cl–Cl distance $r=3.90$ bohr, and a Cl–M (M: the Cl₂ center-of-mass) distance $R=8.70$ bohr. The bent asymmetric minimum ($\tilde{\mathbf{X}}'\mathbf{B}$) is of ${}^2A'$ symmetry, with $r=3.90$ bohr, $R=6.85$ bohr, and the angle between \hat{r} and \hat{R} , $\gamma=68.4^\circ$. Spin-orbit CI (configuration interaction) predicts that the global minimum is linear $\tilde{\mathbf{X}}\mathbf{L}$ (${}^2\Pi_{3/2}$) with a bond dissociation energy of $D_e(\text{Cl}_2(X)-\text{Cl})$ of 280 cm^{-1} . Low-lying doublet excited states have only one strongly bound structure, a linear symmetric $\tilde{\mathbf{A}}\mathbf{L}$ (${}^1{}^2\Pi_g$) state with a bond distance of 4.67 bohr. This state is bound by $\sim 4300\text{ cm}^{-1}$ with respect to the $\text{Cl}_2({}^3\Pi_u)+\text{Cl}$ asymptote, and its minimum lies about 8700 cm^{-1} above the $\tilde{\mathbf{X}}\mathbf{L}$ van der Waals minimum. Transition dipole moment calculations show that the $\tilde{\mathbf{A}}-\tilde{\mathbf{X}}$ transition is fully allowed. Two bound quartet minima were located. The most deeply bound was $\tilde{\mathbf{QD3h}}$ (${}^1{}^4A_1'$) with a D_{3h} equilibrium geometry ($r=5.00$ bohr) about $11\,300\text{ cm}^{-1}$ above $\tilde{\mathbf{X}}\mathbf{L}$. The other state, $\tilde{\mathbf{QC2v}}$ (${}^1{}^4A_2$) had a C_{2v} equilibrium geometry ($r_1=4.83$ bohr and $\theta=101.7^\circ$) and an energy of about $13\,500\text{ cm}^{-1}$ relative to $\tilde{\mathbf{X}}\mathbf{L}$. Although $\text{Cl}_3(\tilde{\mathbf{X}})$ is shown to be unstable, the present results support the notion that Cl₃ participates in Cl atom recombination processes. However, the energies and transition moments of the low-lying excited states are not consistent with electronic spectra that have been tentatively assigned to Cl₃. © 1998 American Institute of Physics. [S0021-9606(98)01507-4]

I. INTRODUCTION

The formation of bound trihalogen intermediates has been proposed to explain a number of kinetic observations.^{1–14} These include the efficiency of X_2 as a third body for halogen atom recombination reactions, and the conservation of atomic electronic angular momentum in $X({}^2P_{1/2})+Y_2\rightarrow XY+Y({}^2P_{1/2})$ exchange reactions.^{3–9} Recently, additional interest in bound trihalogens has been generated by time-resolved studies of the $\text{Br}({}^2P_{1/2})+\text{I}_2$ reaction.^{10–14} Despite the accumulated indirect evidence for the existence of bound trihalogens, there have been very few spectroscopic observations of these species. Fluorine containing trihalogens have been observed in rare-gas matrices by IR (infrared) absorption techniques.^{15–19} Br₃ has been detected by mass spectrometry.²⁰ Otherwise, attempts to observe homonuclear trihalogens have yielded uncertain results.^{21–24} There have been tentative sightings of IR²¹ and visible^{22–24} spectra for Cl₃, but the data obtained have not been suitable for unambiguous identification of the carrier. The present theoretical study was undertaken to predict the ground-state structure and stability of Cl₃, and to predict the characteristics of low-lying electronic transitions. These data have been used to assess the likelihood that the tentatively assigned spectra originate from Cl₃. Before describing our results, we briefly summarize the previous work on Cl₃.

Hutton and Wright² proposed a mechanism for Cl atom

recombination in the presence of Cl₂ that involved the reactions



Hutton and Wright² searched for the electronic absorption spectrum of Cl₃ in the 220–800 nm range, but they were unsuccessful. This was not a particularly troubling result, as the absorption techniques they used were not very sensitive, and Cl₃ would have been present in low concentrations in their experiments. A few years later, Nelson and Pimentel²¹ tried to isolate Cl₃ in cryogenic rare-gas matrices. A microwave discharge was used to generate transient species in Ar/Cl₂ or Kr/Cl₂ gas flows, and the products were deposited on a cold window. An IR absorption spectrum was found in the Kr matrix that was attributed to Cl₃, slightly perturbed by an asymmetric cage. However, subsequent matrix work by Wight *et al.*²⁵ showed that the species observed by Nelson and Pimentel²¹ was ionic, and most probably the Cl₃[−] anion.

A variety of theoretical methods have been used to compute equilibrium structures and potential energy surfaces for Cl₃.^{26–33} One of the most accurate and informative *ab initio* calculations was performed by Sannigrahi and Peyerimhoff.²⁶ Guided by the results of Nelson and Pimentel,²¹ these authors investigated $D_{\infty h}$ and C_{2v} structures. Under these constraints they obtained a bent $\tilde{\mathbf{X}}{}^2A_1$

ground state with a bond length of 4.2 bohr and a bond angle of 146° .

Although most studies seemed to indicate that ground-state Cl_3 was a significantly bound species, there was one indication that it might be unstable. Lee *et al.*³⁴ used crossed molecular beams to study $\text{Cl}_2 + \text{Cl}$ collisions. Their analysis of the scattering distribution was consistent with a weak Cl_2 -Cl bond strength of about 330 cm^{-1} . In other gas-phase studies it was assumed that Cl_3 was stable enough that observable concentrations could be generated at room temperature. Kawasaki *et al.*²² reported an intriguing new laser induced fluorescence (LIF) spectrum of a species formed by photolysis or microwave discharge of Cl_2 . The excitation spectrum appeared in the 415–427 nm range, and the fluorescence was strongest at near-resonant wavelengths. The fluorescence decay lifetime was long ($\tau > 12 \mu\text{s}$), indicative of a metastable excited state. The species responsible for this spectrum appeared to be rather stable, as the LIF signal persisted for several minutes after the photolysis source was turned off. Based on their observations, and the results of a theoretical calculation,³⁵ Kawasaki *et al.*²² tentatively assigned the LIF spectrum to an electronic transition of Cl_3 originating from the \tilde{X}^2A_1 ground state. In similar experiments, Wright *et al.*²³ observed a broad-band, low-level emission in the 370–440 nm region when they photolyzed relatively high pressure (≈ 400 Torr) samples of Cl_2 . Following the work of Kawasaki *et al.*²² they suggested that their spectrum may also originate from Cl_3 , and performed new *ab initio* calculations to explore this possibility.^{23,36} Wright *et al.*^{23,36} approximately reproduced the results of Sannigrahi and Peyerimhoff²⁶ for C_{2v} structures. In addition, they examined asymmetric geometries. For the ground state they found a linear asymmetric van der Waals minimum that was at a much lower energy than the C_{2v} minimum. They concluded, however, that the C_{2v} structure was a stable ground-state minimum (real vibrational frequencies were predicted for all three vibrational modes).

Most recently, Lawrence *et al.*²⁴ searched for the electronic absorption and emission spectra of matrix isolated Cl_3 . In this study, *in situ* photolysis of $\text{HCl}-\text{Cl}_2$ dimers in an Ar matrix was used to generate Cl_3 . After photolysis, near uv excitation of the matrices (305–320 nm) produced a strong blue emission. Dispersed fluorescence spectra revealed a single broad peak, centered at 470 nm. The fluorescence was emitted with a lifetime of $44 \pm 2 \mu\text{s}$ at 12 K. The characteristics of this emission were consistent with the gas-phase spectrum of Kawasaki *et al.*²² when the usual matrix effects were taken into account. This similarity and other circumstantial evidence was used to provisionally assign the matrix spectrum to Cl_3 .

In the present theoretical study we have found that the weakly bound van der Waals structure is the true ground-state minimum for Cl_3 , and that the \tilde{X}^2A_1 structure is not stable. Despite the weakness of the attractive forces, an approximate statistical model of the equilibrium represented by reaction (1) supports the notion that transient formation of Cl_3 participates in the recombination kinetics.² The energies and well-depths of low-lying excited states (including ion-pair states) have been predicted in hopes of finding assign-

ments for the visible and near uv (ultraviolet) spectra described above. Metastable states that could be responsible for emissions in the 400–500 nm region were not found. This result, taken with the low stability of ground state, casts serious doubt on all of the tentative spectroscopic observations of Cl_3 .

Near the completion of the present work, we learned of new calculations for $\text{Cl}_3(\tilde{X})$ from Galbraith *et al.*³⁷ This group used both *ab initio* [CCSD and CCSD(T)] and density functional (BHLYP, B3LYP, and B3P86) methods to explore the ground state. Their results are in general agreement with ours, and they noted that the symmetric \tilde{X}^2A_1 structure was not stable when problems associated with low-lying excited states and/or symmetry breaking were corrected.

II. DETAILS OF CALCULATIONS

The *ab initio* quantum chemistry package MOLPRO96³⁸ was used to perform the calculations in this study, unless otherwise specified. AO (atomic orbital) basis sets were chosen so that the best description of excited states could be obtained. Dunning's³⁹ correlation consistent valence double (*avdz*), triple (*avtz*), and for Cl_2 , quadruple zeta (*avqz*) basis sets were employed. These included a number of polarization and diffuse functions. Unless otherwise specified, the *avdz* basis set was used throughout the paper. Spherical harmonic gaussian basis functions (e.g., five *d* functions) were used in MOLPRO calculations.

In the CASSCF⁴⁰ calculations, the $1s2s2p$ inner shells were kept doubly occupied but fully optimized. The active space consists of the $3s3p$ shells of chlorine atoms, and hence contains all the configurations arising from 21 electrons distributed among 12 molecular orbitals. This gives rise, on the average, to 150 CSF's (configurational state functions) in the CASSCF (complete active space self-consistent field) method. CASSCF-(IC)-MRSDCI, CASSCF-(IC)-CASPT2, and RCCSD (restricted coupled-cluster singles and doubles) methods were used to treat electron correlation in the system. For many regions of the Cl_3 potential-energy surface, internally contracted (IC) multireference single and double configuration interaction⁴¹ (MRSDCI) was used on the CASSCF wave function, to treat electron correlation in the system. This computationally expensive method is always a good treatment for a relatively small system such as Cl_3 . An analog of Davidson's quadruple correction⁴¹ for approximate size-consistency was always included in (IC)MRSDCI. The reference space for MRSDCI was as follows: $1s2s2p$ were frozen and, therefore, always doubly occupied; $3s$ was doubly occupied, but all possible single and double excitations were taken from it, and $3p$ was open. This led to approximately 5×10^7 uncontracted and 10^6 contracted configurations. The reference space for CASPT2 (complete active space second-order perturbation theory)⁴² was similar to that of MRSDCI except that the $3s$ shell was not held doubly occupied. All relative energies were obtained without the counterpoise correction⁴³ (CPC) for basis set superposition error (BSSE), unless specifically mentioned.

Two coordinate systems were used to represent Cl_3 . As will be discussed later, the low-lying states of Cl_3 were found

TABLE I. Summary of equilibrium distance r_e (bohr) and binding energy D_e (cm^{-1}) of Cl_2 valence states.

Method State	CASSCF		MRSDCI			Expt. ^a
	<i>avdz</i>	<i>avtz</i>	<i>avdz</i>	<i>avtz</i>	<i>avqz</i>	
$X^1\Sigma_g^+$	r_e	3.90	3.90	3.90	3.82	3.75
	D_e	12 000	13 000	15 500	19 000	20 277.3
$1^3\Pi_u$	r_e	6.5	6.5	4.9	4.77	4.60 ^b
	D_e	200	200	2,000	2,500	
$1^1\Pi_u$	r_e	repulsive	repulsive	6.60	6.50	
	D_e	0	0	150	190	

^aTaken from Ref. 45.^bFor $^3\Pi(0_u^+)$.

to be repulsive, or they corresponded to weakly bound van der Waals complexes between a Cl_2 molecule and a $\text{Cl}(^2P)$ atom. For this situation the molecule is most suitably represented by the Jacobi coordinates r , R , and γ , where r is the Cl_2 internuclear separation, R is the distance from the Cl_2 molecule center of mass to the $\text{Cl}(^2P)$ atom, and γ is the angle between the vectors \hat{r} and \hat{R} . Some of the excited states were more strongly bound, and had equilibrium geometries with C_{2v} , $D_{\infty h}$, or D_{3h} symmetry. For these states it was more convenient to use valence coordinates, denoted by the two bond lengths r_1 and r_2 and the bond angle θ .

III. Cl_2 POTENTIAL-ENERGY CURVES

A rigorous MRDCI study of Cl_2 by Peyerimhoff and Buenker⁴⁴ described all the valence states, charge-transfer states, and some of the Rydberg states of the molecule. From experimental data⁴⁵ and this theoretical study, it has been established that the only bound valence states of Cl_2 are the $X^1\Sigma_g^+$ and $1^3\Pi_u$ states. Hence, it is most likely that the states of Cl_3 that could be observed in a room-temperature experiment would correlate with Cl_2 ($X^1\Sigma_g^+$, $1^3\Pi_u$) interacting with a chlorine atom (2P_u).

In order to choose the optimal basis set for CASSCF and MRSDCI calculations of Cl_3 , we performed calculations for the ground $X^1\Sigma_g^+$ and the first excited states, $1^3\Pi_u$ and $1^1\Pi_u$, of Cl_2 , whose accurate spectroscopic data are available in the literature. The reason for including the $1^1\Pi_u$ state in the calculation is its indirect participation in low-lying excited-state potential surfaces, since avoided crossings

were expected between the states arising from $\text{Cl}_2(1^1\Pi_u) + \text{Cl}$ and $\text{Cl}_2(1^3\Pi_u) + \text{Cl}$ asymptotes. The major electronic configurations for the three states of Cl_2 near the ground-state equilibrium distance are

$$X^1\Sigma_g^+ : [3p\sigma_g^2\pi_u^4\pi_g^*4\sigma_u^*0]$$

$$1^3\Pi_u, 1^1\Pi_u : [3p\sigma_g^2\pi_u^4\pi_g^*3\sigma_u^*1]$$

CASSCF-MRSDCI and CASSCF calculations were performed to determine the binding energies and equilibrium internuclear separations of these lowest-lying states. The results are summarized in Table I, which clearly shows that the CASSCF method with the *avdz* basis set is needed to reproduce the qualitative behavior of the potential-energy curves. For better energetics, the MRSDCI method with the *avtz* basis set was needed. The improvement of using *avqz* over *avtz* is rather small. Based on these test results, we decided to use mainly CASSCF and MRSDCI for Cl_3 , with the *avdz* basis set for surveys of the potential-energy surfaces, and MRSDCI/*avtz* for some single point energies.

IV. STATES OF Cl_3 CORRELATING WITH THE $\text{Cl}_2(X^1\Sigma_g^+) + \text{Cl}(^2P_u)$ DISSOCIATION LIMIT

A. Linear geometries

First we consider collinear approach of $\text{Cl}(^2P_u)$ to $\text{Cl}_2(X^1\Sigma_g^+)$. The interaction with Cl_2 breaks the atomic orbital degeneracy, giving rise to a $^2\Pi$ state and a $^2\Sigma^+$ state. The major electronic configurations for these states near the asymmetric potential energy minimum, and for symmetric ($D_{\infty h}$) structures are

$C_{\infty v}$	$D_{\infty h}$
$^2\Pi : [3p\sigma^2\pi^4\pi^*4\sigma^2\pi^3\sigma^*0]$	$^2\Pi_u : [3p\sigma_u^2\pi_u^4\pi_g^*4\sigma_g^2\pi_u^3\sigma_u^*0]$
$^2\Sigma^+ : [3p\sigma^2\pi^4\pi^*4\sigma\pi^4\sigma^*0]$	$^2\Sigma_g^+ : [3p\sigma_u^2\pi_u^4\pi_g^*4\sigma_g\pi_u^4\sigma_u^*0]$

(the $C_{\infty v}$ and $D_{\infty h}$ symmetries are treated as C_{2v} and D_{2h} in the calculations). Figure 1 shows CASSCF potential-energy contour plots for the $\tilde{X}^2\Pi$ and $1^2\Sigma^+$ states as functions of the two bond distances, r_1 and r_2 . These plots illustrate qualitative features of the surfaces.

MRSDCI calculations indicate that the $1^2\Sigma^+$ surface

lies entirely above the $\text{Cl}_2(X^1\Sigma_g^+) + \text{Cl}(^2P_u)$ dissociation asymptote, while the $\tilde{X}^2\Pi$ state is slightly bound. Numerical optimization of the MRSDCI energy (without CPC) located the linear minimum (designated as $\tilde{X}\text{L}$ in the following) at $r_e = 3.906$ bohr and $R_e = 8.47$ bohr. The optimized r_e value was only 0.003 bohr longer than the calculated equilibrium

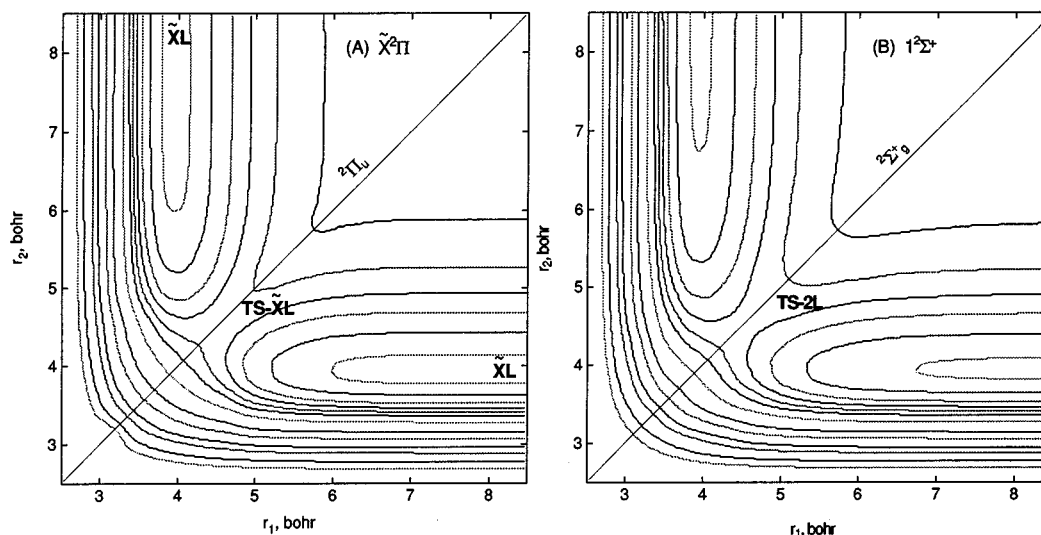


FIG. 1. Potential-energy surfaces (in cm^{-1} , relative to $\text{Cl}+\text{Cl}+\text{Cl}$) for collinear $\text{Cl}\cdots\text{Cl}\cdots\text{Cl}$ structures of Cl_3 , as functions of two bond distances, in the (A) $\tilde{X}^2\Pi$ and (B) $1^2\Sigma^+$ states, at the CASSCF level. The structure $\tilde{X}\mathbf{L}$ is the true minimum and corresponds to the van der Waals complex. The symmetric structures $\text{TS-}\tilde{X}\mathbf{L}$ ($\tilde{X}^2\Pi_u$) and $\text{TS-}2\mathbf{L}$ ($1^2\Sigma_g^+$) are saddle points for Cl exchange. The six lowest contours for both (A) and (B) are at $-10\,848$, -9092 , -7117 , -5361 , -3386 , and -1191 cm^{-1} .

diatomic distance ($r_e = 3.903$ bohr) for $\text{Cl}_2(X)$. The binding energy of $\tilde{X}\mathbf{L}$, including the full counterpoise correction for BSSE, was 250 cm^{-1} . Calculations for bent geometries, as will be shown later, indicate that $\tilde{X}\mathbf{L}$ has a positive bending force constant and is the only true minimum for a linear structure on the ground-state surface. The asymmetric geometry and the small interaction energy indicate $\tilde{X}\mathbf{L}$ corresponds to a $\text{Cl}-\text{Cl}_2$ van der Waals complex. For the optimized geometry, an MRSDCI/*avtz* calculation gave a binding energy of 380 cm^{-1} . Estimating a BSSE correction of about $50\text{--}70\text{ cm}^{-1}$ (extrapolated from the *avdz* value of $\sim 100\text{ cm}^{-1}$), the CP corrected value should predict a binding energy of $300\text{--}320\text{ cm}^{-1}$.

It was shown by Sannigrahi and Peyerimhoff²⁶ that, at the linear symmetric ($D_{\infty h}$) stationary point, $1^2\Sigma_g^+$ and the A'' Renner-Teller component of the $\tilde{X}^2\Pi_u$ state are bound with respect to both bending and symmetric stretch. Our calculations yield similar results. For example, we find that $\tilde{X}^2\Pi_u$ and $1^2\Sigma_g^+$ are bound, at the MRSDCI level, by $11\,500$ and $11\,250\text{ cm}^{-1}$ with respect to the $\text{Cl}+\text{Cl}+\text{Cl}$ dissociation asymptote. Because the experimental data available at the time indicated a symmetric geometry for $\text{Cl}_3(\tilde{X})$, Sannigrahi and Peyerimhoff²⁶ did not examine the behavior of the asymmetric stretch. Based on the potentials for symmetric displacements, they concluded that Cl_3 was a stable species. However, our MRSDCI calculations clearly show that the $\tilde{X}^2\Pi_u$ and $1^2\Sigma_g^+$ states are unstable with respect to asymmetric displacements. It should be noted that the A'' component of $\tilde{X}^2\Pi_u$ does exhibit a local minimum, but the barrier to escape from this minimum is only 44 cm^{-1} . This local minimum is not evident in the CASSCF calculations as they were unable to show such small energy differences. Instead, Fig. 1(A) shows a rather a flat region around the stationary point. The symmetric structures are linear transition states for the Cl atom exchange reaction

$\text{Cl}+\text{Cl}_2 \rightarrow \text{Cl}_2+\text{Cl}$. Consequently, they are labeled as $\text{TS-}\tilde{X}\mathbf{L}$ ($\tilde{X}^2\Pi_u$) and $\text{TS-}2\mathbf{L}$ ($1^2\Sigma_g^+$).

B. Bent van der Waals structures

Upon bending the orbital degeneracy of the $\tilde{X}^2\Pi$ state is lifted, and the symmetry of $1^2\Sigma^+$ is lowered. The correlations between the irreducible representations for linear and bent geometries are,

linear, $C_{\infty v}$	bent, C_s	T-shaped, C_{2v}
$\tilde{X}^2\Pi_y$	\tilde{X}^2A'	\tilde{X}^2A_1
$\tilde{X}^2\Pi_x$	$1^2A''$	1^2B_1
$1^2\Sigma^+$	$2^2A'$	1^2B_2

Figure 2(A) shows a contour plot of the potential energy for the \tilde{X}^2A' state calculated at the MRSDCI+CPC level, as a function of the position of the Cl atom. For this plot the origin is the Cl_2 midpoint, and the Cl_2 distance was fixed at 3.90 bohr (approximately the optimized value). Two minima are evident in Fig. 2(A); one is the linear van der Waals complex $\tilde{X}\mathbf{L}$ described above, and the other is a bent complex $\tilde{X}'\mathbf{B}$ also having typical van der Waals characteristics. MRSDCI optimization gave geometrical parameters for $\tilde{X}'\mathbf{B}$ of $r_e = 3.901$, $R_e = 6.85$ bohr, and $\gamma_e = 66.47^\circ$. As for the $\tilde{X}\mathbf{L}$ minimum, the diatomic distance was barely perturbed by the interaction with the Cl atom. There are two saddle points on the \tilde{X}^2A' surface shown in Fig. 2(A). The saddle point $\text{TS-}\tilde{X}'\mathbf{LB}$ is the transition state connecting the linear minimum $\tilde{X}\mathbf{L}$ and the bent minimum $\tilde{X}'\mathbf{B}$. The T-shaped (C_{2v} , $\gamma = 90^\circ$) saddle point $\text{TS-}\tilde{X}'\mathbf{BB}$ connects the bent minimum at angle γ_e with its counterpart at $180^\circ - \gamma_e$. The energies of the two saddle points are very similar ($\approx -180\text{ cm}^{-1}$) relative to the dissociation limit. Therefore,

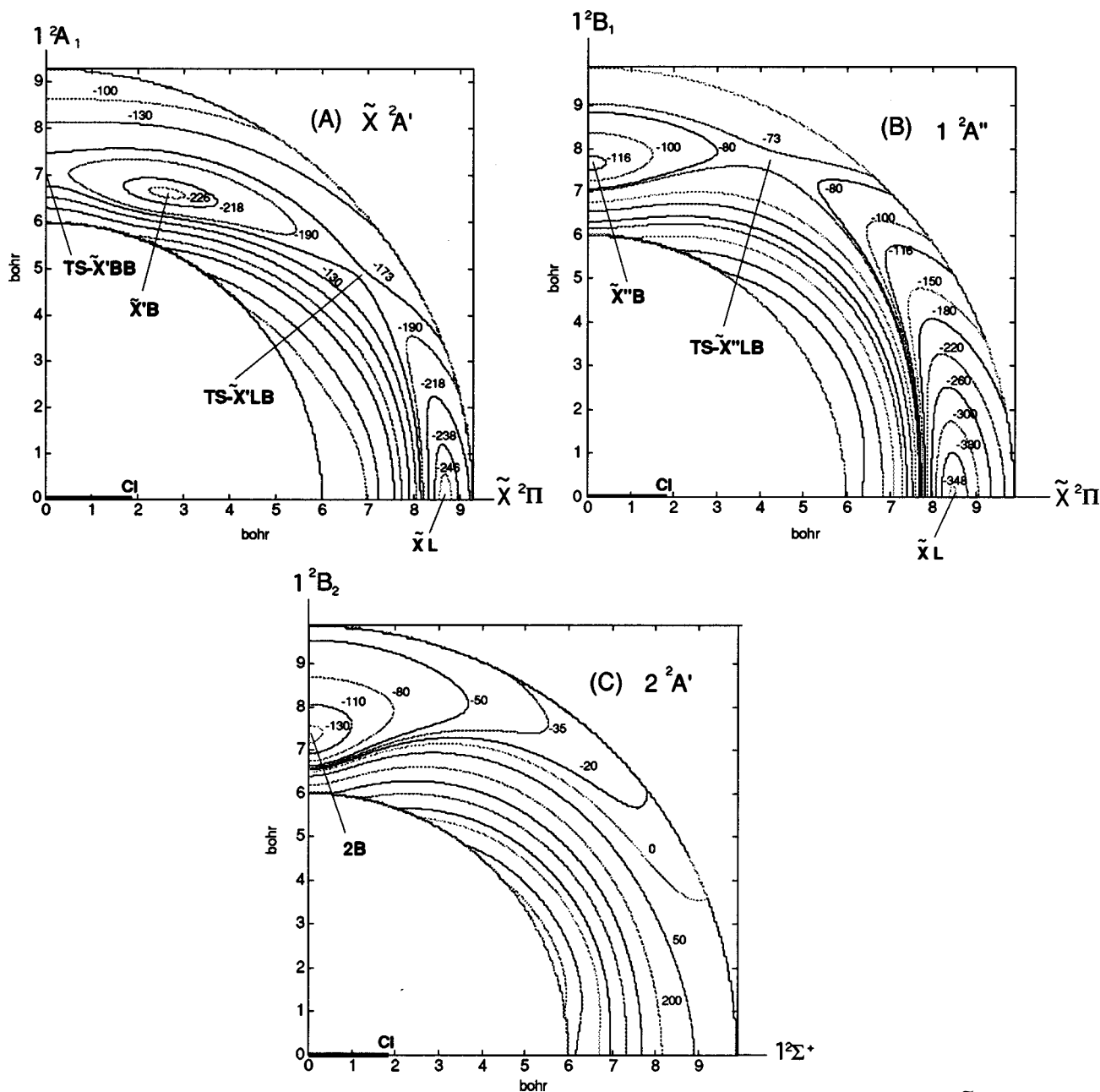


FIG. 2. Potential-energy surfaces [in cm^{-1} with CPC, relative to $\text{Cl}_2(X) + \text{Cl}$ for bent van der Waals $\text{Cl}_2 \cdots \text{Cl}$ structures of Cl_3 , for (A) \tilde{X}^2A' at the MRSDCI level, (B) $1^2A''$ and (C) $2^2A'$ states, at the CASPT2 level (note that the linear minimum is deeper at the CASPT2 level). The Cl_2 center of mass is placed at the origin, so the Cl atom shown on the abscissa appears at half the bond length ($r/2=1.95$ bohr)]. The structure $\tilde{X}'B$ is the true bent minimum and a van der Waals complex. $\tilde{X}L$ is the linear minimum of Fig. 1. The structure $\text{TS-}\tilde{X}'LB$ and $\text{TS-}\tilde{X}'BB$ on \tilde{X}^2A' are saddle points connecting the two minima, $\tilde{X}'B$ and $\tilde{X}L$ and $\tilde{X}B$ and $\tilde{X}B'$, respectively. $\tilde{X}''B$ and $2B$ are T-shaped minima on the $1^2A''$ and $2^2A'$ states, respectively.

the lowest bending vibrational levels should be localized around $\tilde{X}L$ or $\tilde{X}'B$. With increasing excitation of the bending mode, the motion will evolve from a large amplitude libration to an hindered internal rotation.

The two minima $\tilde{X}'B$ and $\tilde{X}L$ have nearly the same energy; the bent minimum was 20 cm^{-1} above or 9 cm^{-1} below $\tilde{X}L$ for calculations with or without CPC, respectively. The counterpoise correction increased the R_e 's of $\tilde{X}'B$ and $\tilde{X}L$ by ≈ 0.3 bohr.

Potential-energy surfaces for the $1^2A''$ and $2^2A'$ states were examined using CASPT2. Before describing the results, a comment on the quality of CASPT2 calculations, as evalu-

ated against MRSDCI results, is in order. For the \tilde{X}^2A' ground state, the CASPT2 potential surface was very similar to the MRSDCI surface. For instance, the CASPT2 bent minimum $\tilde{X}'B$ was found at $r_e=3.91$ bohr, $R_e=6.67$ bohr, $\gamma_e=68.3^\circ$. These coordinates, and the binding energy of 367 cm^{-1} , compare favorably with the MRSDCI results in Table II. Considering its much lower cost ($\sim 1/10$) and size-extensivity, CASPT2 is an excellent method for ground-state van der Waals interactions. It is not as accurate in predicting excitation energies or potential-energy surfaces for excited states with strong configuration interaction.

CASPT2 potential surfaces for the $1^2A''$ and $2^2A'$

TABLE II. Summary of equilibrium and transition state structures and energies on the Cl₃ potential-energy surfaces.^a

Method Structure	MRSDCI				CASPT2				MRSDCI/avtz			
	Energy ^b	<i>r</i>	<i>R</i>	γ	Energy ^b	<i>r</i>	<i>R</i>	γ	Energy ^c	<i>r</i>	<i>R</i>	γ
Cl ₂ ($X^1\Sigma_g^+$) + Cl	0.0	3.90			0.0	3.90			0.0	3.82		
$\tilde{\mathbf{X}}\mathbf{L}$ ($\tilde{X}^2\Pi$)	-249	3.90	8.70	180.0					-380	3.82	8.45	180.0
$\tilde{\mathbf{X}}'\mathbf{B}$ (\tilde{X}^2A')	-228	3.90	7.11	68.4								
TS-$\tilde{\mathbf{X}}'\mathbf{B}\mathbf{B}$ (\tilde{X}^2A')	-185	3.90	7.06	90.0								
TS-$\tilde{\mathbf{X}}'\mathbf{L}\mathbf{B}$ (\tilde{X}^2A')	-173	3.90	8.44	35.4								
$\tilde{\mathbf{X}}''\mathbf{B}$ (1^2B_1)					-118	3.91	7.66	90.0				
TS-$\tilde{\mathbf{X}}''\mathbf{L}\mathbf{B}$ ($1^2A''$)					-75	3.90	8.78	61.3				
2B (1^2B_2)					-133	3.91	7.36	90.0				
Structure	Energy ^c	<i>r</i> ₁	<i>r</i> ₂	θ	Energy ^c	<i>r</i> ₁	<i>r</i> ₂	θ	Energy ^c	<i>r</i> ₁	<i>r</i> ₂	θ
TS-$\tilde{\mathbf{X}}'\mathbf{V}$ (\tilde{X}^2A_1)	1822	4.27	4.27	145.2					1612	4.16	4.16	145.9
TS-$\tilde{\mathbf{X}}\mathbf{L}$ ($\tilde{X}^2\Pi_u$)	4377	4.36	4.36	180.0								
TS-2L ($1^2\Sigma_u^+$)	5026	4.40	4.40	180.0								
Cl ₂ ($^3\Pi_u$) + Cl	13 000	4.90							16 500	4.77		
Cl ₂ ($^1\Pi_u$) + Cl	15 350	6.60							18 810	6.50		
$\tilde{\mathbf{A}}\mathbf{L}$ ($1^2\Pi_g$)	8662	4.67	4.67	180.0					9735	4.54	4.54	180.0
QD3h ($1^4A_1'$)	11 056	5.00	5.00	60.0	7778	4.85	4.85	60.0	11 566 ^d	4.92 ^d	4.92 ^d	60.0 ^d
QC2v (1^4A_2)	13 214	5.12	5.12	100.5	11 115	4.83	4.83	101.7				

^aAll distances are given in bohr, angles in degrees and relative energies in wave numbers.

^bCP corrected.

^cCP uncorrected.

^dCCSD/avdz; $r_e(\text{Cl}_2) = 3.88$.

states are shown in Figs. 2(B) and 2(C), respectively. The linear minimum of $1^2A''$ is the antisymmetric Renner–Teller component of $\tilde{\mathbf{X}}\mathbf{L}$. There is a shallow secondary minimum $\tilde{\mathbf{X}}'\mathbf{B}$ (1^2B_1) on the $1^2A''$ surface in C_{2v} geometry with $R = 7.8$ bohr. The $2^2A'$ state also has a shallow minimum **2B** (1^2B_2) in a C_{2v} geometry with $R = 7.5$ bohr. The binding energies of these minima are about 118 and 133 cm⁻¹, respectively, relative to the Cl₂–Cl asymptote. Both are shallower than the two minima, $\tilde{\mathbf{X}}\mathbf{L}$ and $\tilde{\mathbf{X}}'\mathbf{B}$ of the ground state.

C. Bent symmetric structures

With Cl₃ constrained to C_{2v} geometries, Sannigrahi and Peyerimhoff²⁶ found that the linear $\tilde{X}^2\Pi_u$ state was subject to a strong Renner–Teller interaction. The upper Renner–Teller component (2B_1) exhibited a linear stationary point (**TS- $\tilde{\mathbf{X}}\mathbf{L}$**) (the results of our calculations for **TS- $\tilde{\mathbf{X}}\mathbf{L}$** were described above in Sec. IV A). The lower Renner–Teller component (2A_1) had a bent stationary point (**TS- $\tilde{\mathbf{X}}'\mathbf{V}$**). Sannigrahi and Peyerimhoff²⁶ reported coordinates of $r_{1e} = r_{2e} = 4.16$ bohr and $\theta_e = 145^\circ$ for **TS- $\tilde{\mathbf{X}}'\mathbf{V}$** . In the present study, we obtained optimized coordinates of $r_{1e} = r_{2e} = 4.38$ bohr and $\theta_e = 146^\circ$ at the CASSCF level of theory. MRSDCI calculations with the avdz basis yielded $r_1 = r_2 = 4.27$ bohr and $\theta = 145.2^\circ$, and the energy of the stationary point was about 2000 cm⁻¹ above the $\tilde{\mathbf{X}}\mathbf{L}$ and $\tilde{\mathbf{X}}'\mathbf{B}$ minima. Increasing the basis set to avtz changed the MRSDCI results to $r_1 = r_2 = 4.16$ bohr and $\theta = 145.9^\circ$, without changing the energy significantly relative to the ground-state minimum. To examine the stability of the stationary point, calculations were performed with small asymmetric displacements of r_1 and r_2 (θ was fixed at 145.9°). Numerical second derivatives of the MRSDCI/avtz energy yielded a normal mode fre-

quency of 14.7i cm⁻¹, confirming the suspicion that the symmetric bent structure is not stable. As expected, **TS- $\tilde{\mathbf{X}}'\mathbf{V}$** is lower in energy than the alternative exchange reaction saddle points **TS- $\tilde{\mathbf{X}}\mathbf{L}$** and **TS-2L**.

D. The effects of spin–orbit coupling on the ground-state surface

The spin–orbit splitting of ground-state Cl(2P) is 881 cm⁻¹, where $^2P_{3/2}$ is the lower energy component. The spin–orbit energy is large compared to the ≈ 300 cm⁻¹ Cl₂+Cl interaction energy (nonrelativistic) near the van der Waals minima. As the bonding interaction is so weak, the projection of the atomic electronic angular momentum (J_a) on the body-fixed axis will be a good quantum number. Here, we will use Ω to label the unsigned value of this projection. As Cl₂(X) approaches, the Cl($^2P_{3/2}$) state splits into $\Omega = 1/2$ and $\Omega = 3/2$ projection states. Cl($^2P_{1/2}$) gives rise to an additional $\Omega = 1/2$ state.

The spin–orbit interaction was represented by the effective one-electron Breit–Pauli Hamiltonian

$$H_{\text{so}} = \left(\frac{\alpha^2}{2}\right) Z_{\text{eff}} \sum_{i,a} \left(\frac{1}{r_{ia}^3}\right) (\mathbf{r}_{ia} \times \mathbf{p}_i) \cdot \mathbf{s}_i, \quad (3)$$

where i and a represent summations over electrons and nuclei, respectively, with the two-electron part of the spin–orbit Hamiltonian neglected. The value for Z_{eff} , 14.898 27, was optimized at the CASSCF level to fit the spin–orbit splitting of Cl(2P). All spin–orbit calculations were performed with the GAMESS96⁴⁶ package. Cartesian Gaussians (e.g., six d functions) were used in GAMESS calculations. A hybrid representation was used for the spin–coupled states. This is most easily described for linear geometries. First, the

usual spin-free MRSDCI calculation (with CPC) was performed to obtain the six energies corresponding to the $\tilde{X}^2\Pi$ and $1^2\Sigma^+$ states. These were used as the diagonal elements in subsequent spin-orbit CI calculations. The spin-orbit matrix elements, which are off-diagonal for this basis set, were calculated using the dominant CASSCF wave function for each spin-free state. The resulting matrix, which may be referred to as MRSDCI[H_{II}]+CASSCF[H_{II}] was diagonalized to obtain the energies including spin-orbit coupling. Potential-energy curves for linear $\text{Cl}_2(X)+\text{Cl}$, calculated with and without spin-orbit coupling, are shown in Fig. 3. Significant mixing of the $\Omega=1/2$ states was evident. All three spin-orbit states show minima in Fig. 3, but $\tilde{X}\text{L}$ $\tilde{X}^2\Pi_{3/2}$, the true linear minimum of the ground state, was the only state that was bound with respect to angular displacements. Inclusion of the spin-orbit coupling had very little effect on the well depth and equilibrium distance of the $\tilde{X}\text{L}$ minimum. The well depth increased from 250 to 280 cm^{-1} , while the bond length increased by just 0.01 bohr.

The effects of spin-orbit coupling on the bent van der Waals minimum $\tilde{X}'\text{B}$ were briefly examined (this was the only nonlinear geometry calculated with the inclusion of spin-orbit coupling). The 228 cm^{-1} well depth predicted by the spin-free calculations was reduced to 106 cm^{-1} when spin-orbit coupling was taken into account. Hence, $\tilde{X}\text{L}$ $^2\Pi_{3/2}$ is the global minimum of the ground-state surface.

$D_{\infty h}$	$2\Sigma_u^+$	$2\Sigma_g^-$	$4\Sigma_g^+$	$4\Sigma_u^-$
$C_{\infty v}$	$2\Sigma^+$	$2\Sigma^-$	$4\Sigma^+$	$4\Sigma^-$
C_{2v}	2B_2	2B_1	4A_1	4A_2
C_s	$^2A'$	$^2A''$	$^4A'$	$^4A''$

A. Linear geometries

To obtain a qualitative overall picture of the $\text{Cl}_2(^3\Pi_u)+\text{Cl}(^2P_u)$ excited states for coordinates in the vicinity the ground-state minimum, a state averaged CASSCF calculation was performed. Included in this calculation were the three states corresponding to the ground-state dissociation limit ($\tilde{X}^2\Pi$ and $1^2\Sigma^+$), the twelve $\text{Cl}_2(^3\Pi_u)+\text{Cl}(^2P_u)$ states, and the six states that correlate with $\text{Cl}_2(^1\Pi_u)+\text{Cl}(^2P_u)$. Figure 4(A) shows the results for all $^2\Pi$ and $2\Sigma^+$ states as functions of r_2 , with r_1 fixed at 4.67 bohr, the CASSCF equilibrium internuclear distance of linear Cl_3 $\tilde{A}\text{L}(1^2\Pi_g)$ (see below). Here it can be seen that, of the excited states, $^2\Pi$ was the only significantly bound state. The results for states of other symmetry species and the quartet states are not shown, but these were all found to be repulsive under the above constraints.

A two-dimensional CASSCF potential-energy surface for linear $^2\Pi$ is shown in Fig. 5. The minimum, $\tilde{A}\text{L}$, occurs at a symmetric geometry that corresponds to $1^2\Pi_g$. As will be discussed later, this minimum occurs due to valence bond interactions. The main electronic configuration is

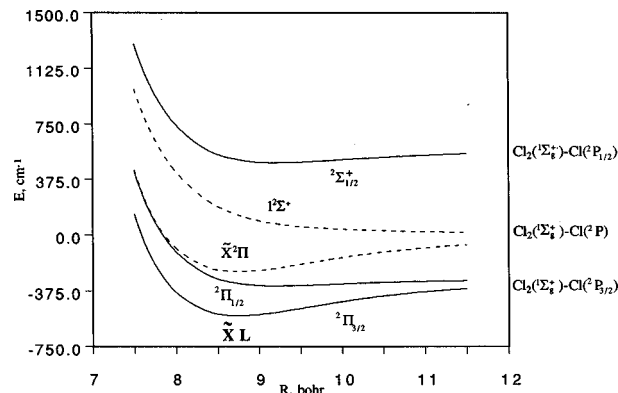


FIG. 3. Potential-energy curves [energy in cm^{-1} relative to the $\text{Cl}_2(X)+\text{Cl}(^2P)$], with (solid curves) and without (broken curves) spin-orbit interaction, at the MRSDCI level. These are for the linear geometry with r_1 fixed at 3.90 bohr. $\tilde{X}\text{L}$ corresponds to the ground-state van der Waals minimum.

V. STATES OF Cl_3 CORRELATING WITH THE EXCITED $\text{Cl}_2(^3\Pi_u, ^1\Pi_u)+\text{Cl}(^2P_u)$ DISSOCIATION LIMITS

There are twelve states that correlate with the $\text{Cl}_2(^3\Pi_u)+\text{Cl}(^2P_u)$ dissociation asymptote. To facilitate discussion of the excited states, it will be helpful to first note the symmetry species of the states for the various geometries considered. The term symbols for these states for the relevant point groups are:

$^2\Pi_g$	$^4\Pi_g$	$^2\Delta_u$	$^4\Delta_g$
$^2\Pi$	$^4\Pi$	$^2\Delta$	$^2\Delta$
$^2A_2, ^2B_2$	$^4A_2, ^4B_2$	$^2A_2, ^2B_2$	$^4A_1, ^4B_1$
$^2A'', ^2A'$	$^4A'', ^4A'$	$^2A'', ^2A'$	$^4A', ^4A''$

$$1^2\Pi_g : [3p\sigma_u^2\pi_u^4\pi_g^*3\sigma_g^2\pi_u^4\sigma_u^*0],$$

representing [$\pi_g^* \rightarrow \pi_u$] excitation from the $\tilde{X}^2\Pi_u$ state.

Starting from a slightly bent symmetric geometry, numerical optimization of the CASSCF energies of the $2^2A''$ and $3^2A'$ states, which correlate with $2^2\Pi$ ($1^2\Pi_g$), gave a linear symmetric geometry with a bond length of 4.93 bohr. Therefore, the linear symmetric structure $\tilde{A}\text{L}$ is a real minimum on the $1^2\Pi_g$ potential surfaces. Both Renner-Teller components were bound for the bending coordinate, indicating that vibronic interaction is small. Optimization of the $2^2\Pi$ state at the MRSDCI level gave a linear symmetric structure $\tilde{A}\text{L}(1^2\Pi_g)$ with bond distances of 4.67 bohr. The MRSDCI/avdz dissociation energy of $\tilde{A}\text{L}$ with respect to $\text{Cl}_2(^3\Pi_u, r_e=4.669 \text{ bohr})+\text{Cl}(^2P_u)$ was 4338 cm^{-1} . Increasing the basis to avtz increased the dissociation energy to 6765 cm^{-1} .

B. Bent geometries

For bent asymmetric geometries there is extensive state mixing within the low-lying manifolds of $^2A'$ and $^2A''$ states.

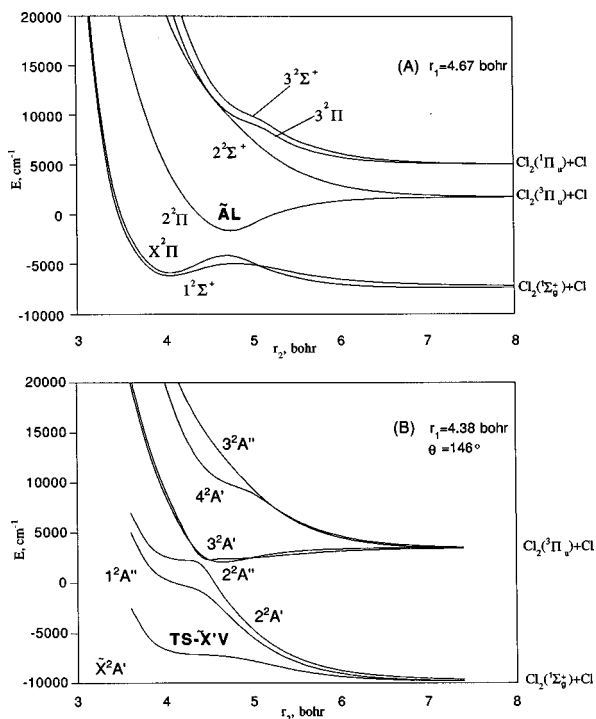


FIG. 4. (A) Potential-energy curves (in cm^{-1} relative to $\text{Cl}_2 + \text{Cl}$) for all $2^2\Sigma^+$ and $2^2\Pi$ states that correlate with $\text{Cl}_2(1^2\Sigma_g^+, 3^2\Pi_u, 1^2\Pi_u) + \text{Cl}(2^2P_u)$. These are for the linear geometry with r_1 fixed at 4.67 bohr. The potentials were obtained from 21-state-averaged CASSCF calculations. (B) Potential-energy curves for bent structures that correlate with $\text{Cl}_2(1^2\Sigma_g^+, 3^2\Pi_u) + \text{Cl}(2^2P_u)$. For these 7-state-averaged CASSCF calculations r_1 and θ were fixed at 4.38 bohr and 146° , respectively.

This point is illustrated by Fig. 4(B), which shows one-dimensional curves calculated with $r_1 = 4.38$ bohr and $\theta = 146^\circ$ (near the symmetric bent transition state $\text{TS-X}'\text{V}$ in the ground state). These curves were obtained from a seven-state-averaged CASSCF calculation. Avoided crossings are evident in this plot in the range $r_2 = 4$ to 5 bohr. Clearly, these avoided crossings and their counterparts in linear geometries [cf., Fig. 4(A)] influence the location of the $2^2\Pi$ state minimum.

CASSCF calculations were used to examine the bending and symmetric stretch modes of the doublet excited states [including those that correlate with $\text{Cl}_2(1^2\Pi_u) + \text{Cl}(2^2P)$]. With the exception of $2^2\Pi$, these states were found to be repulsive.

Quartet states all lowered their energies towards strongly bent geometries. A CASSCF optimization for the lowest $4^2A'$ and $4^2A''$ states in C_s symmetry, near a D_{3h} geometry, led to dissociation. As the three unpaired electrons in these states occupy antibonding orbitals, dynamical correlation is needed to create a bonding interaction. CASPT2 calculations predict that some of the quartet states are bound. For instance, Fig. 6(A) shows CASPT2 potential curves for Cl_3 confined to a D_{3h} geometry. The lowest energy $1^4A_1'$ state seems to be strongly bound and some other states weakly bound, with respect to the $\text{Cl} + \text{Cl} + \text{Cl}$ dissociation limit.

CASPT2 numerical geometry optimizations confirmed that the D_{3h} minimum of $1^4A_1'$ is, in fact, the global minimum for this state (QD3h). The dominant configuration of

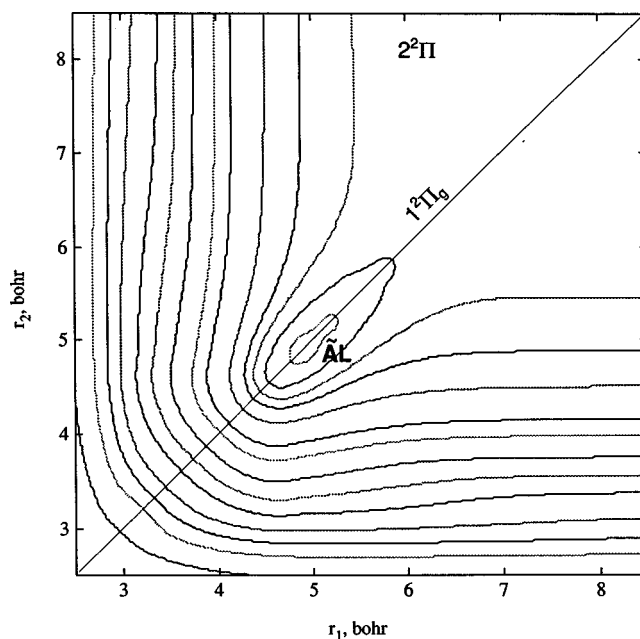


FIG. 5. Potential-energy surface (in cm^{-1} , relative to $\text{Cl}_2(3^2\Pi_u) + \text{Cl}$) of the linear $2^2\Pi$ state. This surface was obtained from a 3-state-averaged CASSCF calculation. The linear symmetric structure AL is a real minimum. The six lowest contours are at -1536 , -658 , 220 , 1098 , 2854 , and 6585 cm^{-1} .

$1^4A_1'$ is $[3pa_1'^2e'^4a_2''^2e''^4e'^2a_2'^1]$. The minimum has a bond length of 4.85 bohr, and $1^4A_1'$ is the lowest energy state in this coordinate region. Optimization of the QD3h bond length using the CCSD⁴⁷ (ACESI⁴⁸ version) analytical gradient technique⁴⁹ yielded $r_e = 4.92$ bohr. Vibrational frequency calculations at the CCSD analytical second derivative⁵⁰ level gave vibrational constants of $\omega_{E'} = 254.5 \text{ cm}^{-1}$ and $\omega_{A_1'} = 308.5 \text{ cm}^{-1}$. These values suggest a rather deep local minimum. However, the MRSDCI energy of this minimum QD3h is $\sim 11\,300 \text{ cm}^{-1}$ above the ground-state van der Waals minimum XL . There was a noticeable disagreement between CASPT2 and MRSDCI energetics of the QD3h minimum, but this was due to the fact that CASPT2 calculates the total energy of Cl_3 ground-state fragments ($\text{Cl}_2 + \text{Cl}$) to be $\sim 4000 \text{ cm}^{-1}$ higher than MRSDCI, relative to the minimum XL . CASPT2 is not expected to do well for excitation energies. On the other hand CCSD, which should be more accurate, calculates the total energy of QD3h to be $\sim 5000 \text{ cm}^{-1}$ higher than the MRSDCI energy. A possible source for this discrepancy is the treatment of the core electrons, which are not frozen during evaluation of CCSD energy derivatives. When a single point calculation is done with the core frozen, the agreement with MRSDCI is very good (cf. Table II).

The $1^4E''$ state, which is derived from partially filled e' and e'' orbitals, is weakly bound when the geometry is constrained to D_{3h} [Fig. 6(A)]. When this state is optimized using CASPT2, the minimum is found to be a C_{2v} structure with $\theta = 101.7^\circ$ and $r_1 = r_2 = 4.83$ bohr (QC2v). The dominant electronic configuration is

$$1^4A_2: [3pa_1^2a_1^2b_2^2b_1^2a_2^2b_1^2b_1^1a_2^1b_2^1].$$

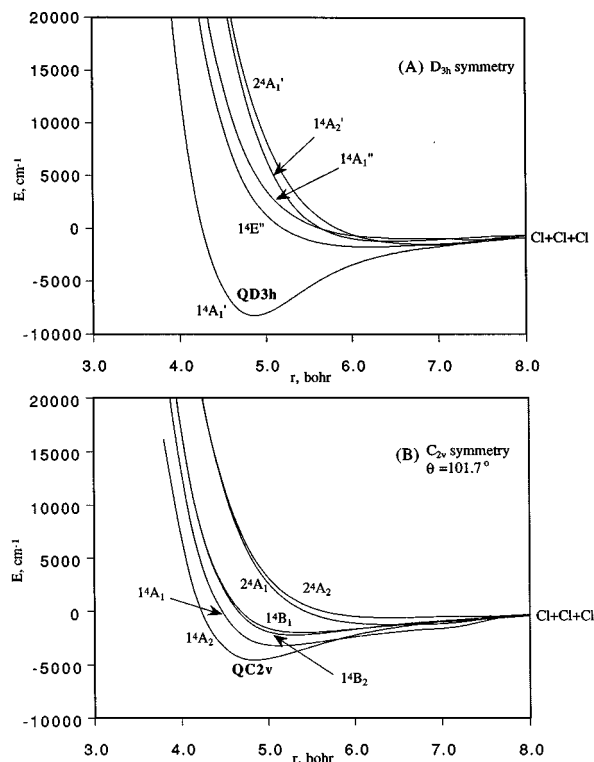


FIG. 6. (A) CASPT2 potential-energy curves (in cm^{-1} with respect to $\text{Cl}+\text{Cl}+\text{Cl}$ limit) of all the quartet states that correlate with $\text{Cl}_2(^3\Pi_u) + \text{Cl}(^2P_u)$. 21-state-averaged CASSCF reference functions were used in calculating this surface. r_1 was fixed at 4.67 bohr. **QD3h** is the lowest true minimum in the quartet state. (B) The same states in C_{2v} , symmetry with the bond angle fixed at 101.7° . **QC2v** is the quartet state.

The MRSDCI energy of (**QC2v**) was about $13\,000\text{ cm}^{-1}$ above the ground-state van der Waals minimum $\tilde{\mathbf{X}}\mathbf{L}$. All other quartet states were predicted to be dissociative.

VI. CHARGE-TRANSFER STATES OF Cl_3

The experimental adiabatic ionization potential of $\text{Cl}_2(X)$ is 11.50 eV ,⁴⁵ and the electron affinity of chlorine atom is 3.61 eV .⁵¹ Consequently, the first charge transfer dissociation asymptote, $\text{Cl}_2^+(X^2\Pi_g) + \text{Cl}^-(^1S_g)$, lies about 8 eV above the van der Waals minimum $\tilde{\mathbf{X}}\mathbf{L}$. For linear geometries, the only state correlating to this limit is a $^2\Pi$ state. From the results of Peyerimhoff and Buenker⁴⁴ and our test calculations on the excited states of Cl_2 , it can be inferred that the maximum number of $^2\Pi$ states, resulting from $\text{Cl}_2 + \text{Cl}(^2P_u)$ interaction, before the first charge-transfer dissociation asymptote occurs, ranges from three to fifteen, depending on the diatomic internuclear distance. A number of state averaged CASSCF calculations were undertaken to find the charge-transfer states. However, in sifting through the $^2\Pi$ states these calculations produced, we were unable to find any that clearly exhibited charge transfer characteristics (e.g., Coulombic long-range attraction).

An approach that involved manipulation of configurations in the MCSCF procedure turned out to be a useful technique for locating the charge transfer states. We first performed a six-state-averaged MCSCF calculation including only three CSF's for electron configuration $(\sigma^2\sigma^2\sigma^*0)$

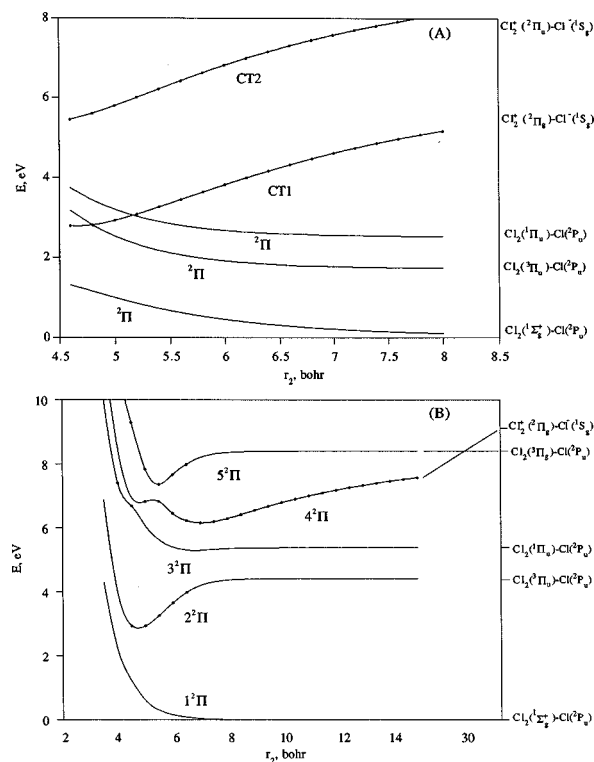


FIG. 7. Potential-energy curves (in cm^{-1} relative to $\text{Cl}_2(^1\Sigma_g^+ + r_e) + \text{Cl}(^2P_u)$) for linear Cl_3 . (A) Diabatic $^2\Pi$ states with r_1 fixed at 3.91 bohr, calculated with a restricted MCSCF. (B) Adiabatic $^2\Pi$ states with r_1 fixed at a smaller value of 3.50 bohr, calculated with five-state-averaged CASSCF. Regions of curves with knots represent substantial contribution of charge-transfer states.

$\times (\pi_x\pi_x\pi_x)^5(\pi_y^2\pi_y^2\pi_y^2)$ and three CSF's for electron configuration $(\sigma^2\sigma^2\sigma^*0)(\pi_x^2\pi_x^2\pi_x^2)(\pi_y\pi_y\pi_y)^5$ to obtain approximate "diabatic" states corresponding to (CT1) $^2\Pi$, and (CT2) $^2\Pi$, where CT1 and CT2 correspond to the $\text{Cl}_2^+(X^2\Pi_g) + \text{Cl}^-(^1S_g)$ and $\text{Cl}_2^+(^2\Pi_u) + \text{Cl}^-(^1S_g)$ dissociation asymptotes, respectively. From a separate MCSCF calculation with a group of six CSF's corresponding to $(\sigma^2\sigma^1\sigma^*0)(\pi_x\pi_x\pi_x)^5(\pi_y^2\pi_y^2\pi_y^2)$ and $(\sigma^2\sigma^1\sigma^*1) \times (\pi_x^2\pi_x^2\pi_x^2)(\pi_y\pi_y\pi_y)^5$, two approximate diabatic $^2\Pi$ states that correspond to $\text{Cl}_2(^3\Pi_u, ^1\Pi_u) + \text{Cl}(^2P)$ limits were obtained. Figure 7(A) shows these four diabatic states and the ground state curve for $r_1 = 3.91$ bohr. As the charge transfer states were not allowed to mix with valence excited states in these calculations, they were easily identified by their long-range behavior.

In general it is difficult to find adiabatic charge-transfer states, since many covalent states are lower in energy and substantial covalent-ionic mixing takes place. For shorter diatomic distances, however, the charge transfer states of Cl_3 drop below many of the covalent states, and may be located in state averaged CASSCF calculations. The calculations of Peyerimhoff and Buenker⁴⁴ and our own results for $r(\text{Cl}_2) \leq 3.5$ bohr predict that there will be no more than three $^2\Pi$ states below the state which dissociates into $\text{Cl}_2^+(X) + \text{Cl}^-(^1S)$. We have performed a five-state-averaged CASSCF calculation (with full valence active space, as in other CASSCF calculations) on the $^2\Pi$ states with the diatomic distance held in the range $r_1 = 3.4\text{--}3.6$ bohr. These

calculations produced some adiabatic states that had substantial ion pair character. Figure 7(B) shows the potential curves for ${}^2\Pi$ states for the very short diatomic distance of $r_1 = 3.5$ bohr. Shown by dots on the potential-energy curves, the charge-transfer contributions derived from the $\text{Cl}_2^+(\text{X}^2\Pi_g) + \text{Cl}^-({}^1S_g)$ asymptote are shared by several adiabatic states and create a series of avoided crossing among them, and no single state can be identified as the ‘‘charge-transfer state’’. Since our approach is limited to linear geometries only, where we can use symmetry very efficiently, we cannot say definitely if these ionic states are true minima. The $5\text{ }^2\Pi$ state, for example, is strongly bound in the stretching motion, but it may become more stable for bent geometries. Transition dipole moments were calculated for $4\text{ }^2\Pi \rightarrow 1,2,3\text{ }^2\Pi$ transitions. For the geometries ranging $r_1 = 3.4\text{--}3.6$ bohr and $r_2 = 5.0\text{--}9.0$ bohr, the transition moment is of the order of 2 a.u.; the transition is very strong, as is expected for a transition containing a charge-transfer character.

VII. PARTICIPATION OF Cl_3 IN THE $\text{Cl} + \text{Cl} + \text{Cl}_2 \rightarrow 2\text{Cl}_2$ RECOMBINATION REACTION

As discussed in the Introduction, Hutton and Wright² proposed a mechanism for the recombination reactions, (1) and (2), involving the triatomic intermediate Cl_3 , and reported rate constants for reaction (1): $\text{Cl} + \text{Cl}_2 \rightleftharpoons \text{Cl}_3$ to be $k_1 = 9.09 \times 10^7 \text{ cm}^3 \text{ mol}^{-1} \text{ s}^{-1}$ (forward) and $k_{-1} \leq 7.6 \times 10^5 \text{ s}^{-1}$ (reverse). These rate constants establish a lower bound for the equilibrium constant of

$$K_{\text{eq}} = \frac{[\text{Cl}_3]}{[\text{Cl}_2][\text{Cl}]} \geq 120 \text{ cm}^3 \text{ mol}^{-1}.$$

We have used the potential-energy surface of the Cl_3 ground state reported here to predict K_{eq} . Application of conventional statistical mechanics to this problem yields

$$K_{\text{eq}} = \frac{q_{\text{Cl}_3}}{q_{\text{Cl}_2} q_{\text{Cl}}} e^{-\Delta U/k_b T}, \quad (4)$$

where the q 's are the molecular partition functions, ΔU is the energy difference between the reactants and products, T is the temperature and k_b is the Boltzman constant. Partition functions for $\text{Cl}({}^2P)$ and $\text{Cl}_2(X)$ are readily evaluated using the accurately known spectroscopic constants. The partition function for Cl_3 was obtained by the following approximate means.

As the van der Waals complex $\tilde{\mathbf{X}}\mathbf{L}$ in $\tilde{\mathbf{X}}\text{ }^2\Pi_{3/2}$ is the only significantly bound state that correlates with $\text{Cl}_2(X) + \text{Cl}({}^2P_{3/2})$, the partition function was calculated based on the properties of this twofold degenerate PES. The vibrational and rotational partition functions were estimated by first noting that $\text{Cl}_2(X)$ is almost unperturbed by the relatively long-range interactions with $\text{Cl}({}^2P_{3/2})$. Hence, the internal motions may be described as the $\text{Cl}_2(X)$ stretch (v_1), the $\text{Cl}_2\text{--Cl}$ van der Waals stretch (v_2), and the $\text{Cl}_2(X)$ internal rotation within the complex. The partition function associated with v_1 was therefore the same as $q_{\text{vib}}(\text{Cl}_2)$.

The van der Waals stretch, internal rotation and overall rotation of Cl_3 were considered in a single partition function

expression [$q_{\text{vdW}}(\text{Cl}_3)$], to ensure that only bound states were included in the summation. The vibrational energies associated with v_2 were calculated using Morse vibrational parameters derived from the radial potential-energy curve shown in Fig. 3. A fit to this curve yielded the vibrational parameters $\omega_e = 40.6$, $\omega_e x_e = 1.68$, $D_e = 245$, and $D_0 = 225 \text{ cm}^{-1}$. To simplify treatment of the internal rotation, the anisotropy of the PES was ignored. For evaluation of the partition function, this should be a reasonably good approximation. The energy level expression for the combined internal rotation and overall rotation could then be written as

$$E(J,L) = bJ(J+1) + BL(L+1), \quad (5)$$

where J and L are the angular momentum quantum numbers for Cl_2 rotation and $\text{Cl}_2\text{--Cl}$ rotation, respectively; b is the $\text{Cl}_2(X)$ rotational constant, and B is the overall rotation constant, obtained by treating Cl_2 as a point mass located at the distance R_e from the Cl atom ($B = 0.036 \text{ cm}^{-1}$). Equation (5) assumes rigid rotor energy expressions for both motions. The van der Waals partition function was defined by

$$q_{\text{vdW}}(\text{Cl}_3) = \sum_{v_2} \sum_J \sum_L \frac{(2J+1)}{2} (2L+1) \times e^{-(E(v_2) + E(J,L))/k_b T}, \quad (6)$$

where division by two accounts for the Cl_2 exchange symmetry and $E(v_2)$ is defined by the usual Morse expression. The summations in Eq. (6) were constrained by the condition $E(v_2) + E(J,L) \leq D_0$. For the well depth obtained from the effective radial potential ($D_0 = -\Delta U = 225 \text{ cm}^{-1}$), Eq. (6) gives $q_{\text{vdW}}(\text{Cl}_3) = 2.0 \times 10^6$ at 295 K. With the above approximations, Eq. (4) predicts an equilibrium constant of $K_e = 40 \text{ cm}^3 \text{ mol}^{-1}$ at 295 K.

VIII. DISCUSSION

A. Ground-state potential-energy surfaces

In contrast to previous studies, we find that the C_{2v} structure for $\text{Cl}_3(\tilde{\mathbf{X}})$ ($\text{TS}\text{--}\tilde{\mathbf{X}}'\mathbf{V}$) is not a true minimum on the ground-state surface. Sannigrahi and Peyerimhoff²⁶ did not examine asymmetric structures and thus did not locate the van der Waals minimum nor identified the C_{2v} structure as a transition state, our C_{2v} structure and energies are in agreement with their earlier high-level calculation. Other lower level calculations have found a minimum for C_{2v} , but the present multireference treatment clearly shows that this geometry is unstable.

The $\text{Cl}_2(X)\text{--Cl}({}^2P_{3/2})$ bond dissociation energy obtained from our calculations (280 cm^{-1}) compares favorably with Lee *et al.* estimate³⁴ of 330 cm^{-1} derived from inelastic scattering data. As was shown in Sec. IV, the dissociation energy of the ground state increased by 100 cm^{-1} or 40% when the *avtz* basis set was used. The dispersion-dominant van der Waals interaction in the ground state requires a very large basis set in order to fully recover the binding energy, so we expect that basis sets of *avqz* quality or better will give even closer agreement with the scattering results. An indirect experimental probe of the $\text{Cl}_2(X)\text{--Cl}$ well depth is provided by the $\text{Cl} + \text{Cl}_2 \rightleftharpoons \text{Cl}_3$ equilibrium constant. In Sec. VII the

equilibrium constant was estimated using the properties of the ground-state PES. The result was about a factor of 3 smaller than the experimental lower bound. Model calculations indicated that the bond dissociation energy needed to be increased to around 600 cm^{-1} in order to obtain agreement with the experimental equilibrium constant. While we had anticipated that the present calculations would underestimate the bond strength, we had not expected that they would be in error by a factor of 2. There are, of course, other possible sources for the discrepancy. These include the simplifications made in estimating the equilibrium constant from the PES, and omissions in the kinetic model used to analyze the original data. Overall, we do not consider the discrepancy to be serious enough to call into question the role of Cl_3 in Cl atom recombination.

It is interesting to note that, for spin-free calculations, the linear van der Waals complex $\tilde{X}^2\Pi$ is lower in energy than the $1^2\Sigma^+$ state. One might think that the least exchange repulsion would be achieved when the unpaired electron approaches the closed shell diatom in the $p\sigma$ orbital, with the $p\pi$ orbitals filled. However, the ground state of Cl_2 has more charge distributed off axis, and the repulsion is smallest when the Cl atom approaches with the $p\sigma$ orbital doubly occupied. For side-on approach the electrostatic and exchange repulsion is minimized when the unpaired electron is in the atomic $p\sigma$ orbital. Hence, the $\tilde{X}B$ van der Waals minimum has A' symmetry.

Geometric aspects of the $\text{Cl}_2(X) + \text{Cl}(^2P_J)$ interactions are not so easily visualized when spin-orbit coupling is included. Dubernet and Hutson⁵² have discussed purely electrostatic interactions between $\text{Cl}_2(X)$ and $\text{Cl}(^2P_J)$. From a general perspective they argued that, for complexes consisting of a 2P atom bound to a closed shell diatom, the $^2P_{3/2}$ state will be much more strongly bound than the $^2P_{1/2}$ state. This situation occurs because there are electrostatic terms for $^2P_{3/2}$ states that are averaged out for $^2P_{1/2}$ states. From Fig. 3 it can be seen that our spin-coupled *ab initio* calculations were in accord with this expectation. Dubernet and Hutson⁵² estimated the anisotropy of the $\text{Cl}_2(X) - \text{Cl}(^2P)$ interaction by assuming that the potential energy would be dominated by the quadrupole-quadrupole term. Their predictions of the relative energies of the ($J_a=3/2, \Omega=3/2$), ($J_a=3/2, \Omega=1/2$), and ($J_a=1/2, \Omega=1/2$) states, for the linear complex with $R=7.4$ bohr (see Fig. 9 of Ref. 45), were in reasonable agreement with the corresponding *ab initio* results. The electrostatic model also predicted a linear equilibrium geometry for the ($J_a=3/2, \Omega=3/2$) ground state. Note that the electrostatic minima of the ($J_a=3/2, \Omega=1/2$) and ($J_a=1/2, \Omega=1/2$) states corresponded to the T-shaped geometry. This was in accord with the fact that the *ab initio* energies for the ($J_a=3/2, \Omega=1/2$) and ($J_a=1/2, \Omega=1/2$) states decreased as the complex was bent away from linear.

B. The Cl exchange saddle points

At the MRSDCI level, barriers to $\text{Cl} + \text{Cl}_2 \rightarrow \text{Cl}_2 + \text{Cl}$ exchange on the ground-state surface were found to be 4377 cm^{-1} (**TS-XL**) and 1822 cm^{-1} (**TS-X'V**). For collinear exchange, Galbraith *et al.*³⁷ obtained a barrier of 4326 cm^{-1}

[CCSD(T)], in excellent agreement with the present result. The barrier to exchange can be understood as originating from an avoided crossing between the two valence bond structures with the odd electron in a $p\pi$ orbital: $\text{Cl}^a - \text{Cl}^b \cdot \text{Cl}^c$ (corresponding to the reactant) and its counterpart $\text{Cl}^a \cdot \text{Cl}^b - \text{Cl}^c$ (corresponding to the product). From Fig. 4(A) it is evident that $2^2\Pi$ is the other state involved in the collinear avoided crossing.

A similar argument applies to the exchange barrier of the $1^2\Sigma^+$ state, as seen also in Fig. 4(A). The saddle point **TS-2L** ($1^2\Sigma_g^+$) is due to the avoided crossing between the two valence bond structures similar to the above but with the odd electron in a σ orbital. This time the interaction is very strong due to the involvement of σ odd electron. Thus the upper state becomes simply repulsive without any minimum, as the interaction is strongly antibonding.

C. Vibrational fundamentals of $\text{Cl}_3(\tilde{X})$

The frequencies of the ground-state stretching modes can be predicted using the MRSDCI potential. As the molecule is basically $\text{Cl}_2(X)$ perturbed by Cl, the high-frequency stretch fundamental will be close to the unperturbed diatomic value of 554.3 cm^{-1} ($^{35}\text{Cl}_2$). From the analysis in Sec. VII, the low-frequency $\text{Cl}_2 - \text{Cl}$ stretch should have its fundamental near 37 cm^{-1} . The bending of Cl_3 has been discussed in some detail by Dubernet and Hutson.⁵² Their analysis of the electrostatic forces appears to be consistent with the *ab initio* results, so it is likely that the bending structure they have calculated is realistic. Their model predicts a bending fundamental of about 10 cm^{-1} . The transition dipoles associated with the three vibrational modes will all be very small, so it would be a difficult matter to observe the IR transitions. The predicted fundamentals are very different from the IR absorption lines reported by Nelson and Pimentel²¹ (e.g., 374.6 cm^{-1} attributed to $^{35}\text{Cl}_3$), reinforcing the notion that they observed something other than Cl_3 .

D. Electronic spectra provisionally assigned to Cl_3

As described in the introduction, broad emission features appearing in the 370–480 nm range have been tentatively assigned to Cl_3 . Measurements in the gas phase and an Ar matrix indicate the emitting levels are long-lived ($\tau > 12\ \mu\text{s}$).^{22,24} Kawasaki *et al.*²² used excitation wavelengths in the range 415–427 nm to obtain their gas-phase emission spectrum. They compared their results with an unpublished *ab initio* calculation³⁵ that predicted absorption transitions at 680 and 370 nm. The transitions were assigned to $1^2B_2 \leftarrow \tilde{X}^2A_1$ and $2^2B_2 \leftarrow \tilde{X}^2A_1$, and the gas-phase spectrum was attributed to the latter. The present calculations predict that vertical $1^2B_2 \leftarrow \tilde{X}^2A_1$ and $2^2B_2 \leftarrow \tilde{X}^2A_1$ transitions will occur near 730 and 450 nm, respectively. The 2^2B_2 state [$4^2A'$ in Fig. 4(B)] does not have bound regions, and will not emit to any significant degree. It is conceivable that the $2^2\Pi - \tilde{X}^2A'$ transition, originating from the van der Waals ground state, could be responsible for the absorption band detected by Kawasaki *et al.*²² However, the emission characteristics of this system would not be consistent with the observations. The transition dipole is relatively small for

the van der Waals geometry, where the transition is approximately $\text{Cl}_2(B^3\Pi) - \text{Cl} - \text{Cl}_2(X) - \text{Cl}$, but the transition dipole becomes large in the vicinity of the $2^2\Pi$ ($1^2\Pi_g$) state minimum. Hence, most transitions would occur in this coordinate region where the Franck–Condon factors will favor strong emission near $2\ \mu\text{m}$. The magnitude of the transition dipole would result in a lifetime of the order of 100 ns.

Bound quartet states that correlate with the $3\text{Cl}(^2P)$ dissociation limit were found in this study, but these cannot account for the gas phase or matrix spectra. Transitions to the bound regions of the quartet surfaces cannot occur at wavelengths shorter than 490 nm (predicated by a ground state well-depth $< 600\ \text{cm}^{-1}$). Lastly, transitions to and from the ion-pair states cannot account for the gas phase or matrix spectra. Starting from $\tilde{\text{X}}\text{L}$ or $\tilde{\text{X}}'\text{B}$, vertical transitions to the ion-pair states (or states with a significant fraction of ion-pair character) will occur at wavelengths shorter than 250 nm (the absorption in the matrix was centered at 320 nm). Emission from the ion-pair states could occur in the 400–500 nm range, but the large transition dipoles would result in short radiative lifetimes ($< 100\ \text{ns}$).

Based on the MRSDCI calculations, we conclude that it is most unlikely that any of the spectra that have been attributed to Cl_3 actually originate from this species.

IX. CONCLUSIONS

We report high-level *ab initio* calculations for the trichlorine radical. CASSCF, (IC)MRSDCI, (IC)CASPT2, CCSD levels of theory were used to explore the potential-energy surfaces of the ground and excited electronic states with (*avdz*) and (*avtz*) basis sets. The ground-state potential surface has two van der Waals complexes, a linear structure $\tilde{\text{X}}\text{L}$ ($\tilde{X}^2\Pi$) and a bent structure $\tilde{\text{X}}'\text{B}$ (\tilde{X}^2A'). The bent symmetric structure $\text{TS}-\tilde{\text{X}}'\text{V}$ (\tilde{X}^2A_1) is a transition state for exchange of a chlorine atom between van der Waals complexes. Of the excited doublet states the linear symmetric structure $\tilde{\text{A}}\text{L}$ ($1^2\Pi_g$) with $r_1 = 4.67$ bohr is the only strongly bound state, located about $8900\ \text{cm}^{-1}$ above the global minimum $\tilde{\text{X}}\text{L}$. Two bound quartet states were found. The most deeply bound quartet state, $1^4A'_1$, had a D_{3h} geometry at the minimum ($\text{QD}3h$; $r = 5.0$ bohr), which was about $11\ 300\ \text{cm}^{-1}$ above $\tilde{\text{X}}\text{L}$. The 1^4A_2 state had a minimum for a C_{2v} geometry ($\text{QC}2v$; $r_1 = 5.12$ bohr and $\theta = 100.5^\circ$) lying about $13\ 500\ \text{cm}^{-1}$ above $\tilde{\text{X}}\text{L}$.

We present evidence that Cl_3 is very unlikely to be responsible for long-lived emissions in 470 nm region. Our calculated potential-energy surfaces do not support the assignment of previously observed visible spectra to Cl_3 . A valence excited state that could emit to a lower-lying state at 470 nm with a long radiative lifetime could not be found. Charge-transfer states were located in almost the “right” region but exhibited very large transition dipole moments (~ 2 a.u.) for emission to lower-lying states, resulting in lifetimes of the order of nanoseconds. Bent structures were not considered for the charge-transfer, but it is unlikely that the conclusions derived from linear structures are changed substantially upon bending.

Our ground-state calculations support the proposed idea that transient Cl_3 formation participates in the process of Cl atom recombination.

ACKNOWLEDGMENTS

We wish to thank the Emerson Center for Scientific Computation for computing facilities and software. The authors also wish to thank Dr. Leonid A. Kaledin for many fruitful discussions. This work was in part supported by the Air Force Office of Scientific Research (F49620-95-1-0010 and F49620-95-1-0182) and the National Science Foundation (CHE 93 20094).

- ¹D. L. Bunker and N. Davidson, *J. Am. Chem. Soc.* **80**, 5090 (1958).
- ²E. Hutton and M. Wright, *J. Chem. Soc. Faraday Trans.* **61**, 78 (1964).
- ³G. E. Hall, W. J. Marinelli, and P. L. Houston, *J. Phys. Chem.* **87**, 2153 (1983).
- ⁴J. I. Cline and S. R. Leone, *J. Phys. Chem.* **95**, 2917 (1991).
- ⁵J. Tellinghuisen and L. F. Phillips, *J. Phys. Chem.* **90**, 5108 (1986).
- ⁶H. K. Haugen, E. Weitz, and S. R. Leone, *Chem. Phys. Lett.* **119**, 75 (1985).
- ⁷H. Hoffman and S. R. Leone, *Chem. Phys. Lett.* **54**, 314 (1978).
- ⁸A. Viste and P. Pyykkö, *Int. J. Quantum Chem.* **25**, 223 (1984).
- ⁹E. B. Gordon, A. I. Nadkhin, S. A. Sotnichenko, and I. A. Boriev, *Chem. Phys. Lett.* **86**, 209 (1982).
- ¹⁰I. R. Sims, M. Gruebele, E. D. Porter, and A. H. Zewail, *J. Chem. Phys.* **97**, 4127 (1992).
- ¹¹M. Gruebele, I. R. Sims, E. D. Porter, and A. H. Zewail, *J. Chem. Phys.* **95**, 7763 (1991).
- ¹²S. A. Wright, M. F. Tuchler, and J. D. McDonald, *Chem. Phys. Lett.* **226**, 570 (1994); M. F. Tuchler, S. A. Wright, and J. D. McDonald, *J. Chem. Phys.* **106**, 2634 (1997).
- ¹³C. Wittig and A. H. Zewail, in *Chemical Reaction in Clusters*, edited by E. Bernstein (Oxford University Press, Oxford, 1995).
- ¹⁴J. C. Polyani and A. H. Zewail, *Acc. Chem. Res.* **28**, 119 (1995).
- ¹⁵G. Mamantov, D. G. Vickroy, E. J. Vasini, T. Maekawa, and M. C. Moulton, *Inorg. Nucl. Chem. Lett.* **6**, 701 (1970).
- ¹⁶G. Mamantov, E. J. Vasini, M. C. Moulton, D. G. Vickroy, and T. Maekawa, *J. Chem. Phys.* **54**, 3419 (1971).
- ¹⁷M. R. Clarke, W. H. Fletcher, G. Mamantov, E. J. Vasini, and D. G. Vickroy, *Inorg. Nucl. Chem. Lett.* **8**, 611 (1972).
- ¹⁸E. S. Prochaska and L. Andrews, *Inorg. Chem.* **16**, 339 (1977).
- ¹⁹E. S. Prochaska, L. Andrews, N. R. Smyrl, and G. Mamantov, *Inorg. Chem.* **17**, 970 (1978).
- ²⁰M. W. Sigrist, D. J. Krajnovich, F. Huisken, Z. J. Zhang, Y. T. Lee, and Y. R. Shen, *Helv. Phys. Acta* **53**, 289 (1980).
- ²¹L. Y. Nelson and G. C. Pimentel, *J. Chem. Phys.* **47**, 3671 (1967).
- ²²M. Kawasaki, H. Sato, and G. Inoue, *J. Phys. Chem.* **93**, 7571 (1989).
- ²³T. G. Wright, A. J. Bell, and J. G. Frey, *Chem. Phys. Lett.* **189**, 297 (1992).
- ²⁴W. G. Lawrence, R. M. Fulghum, and M. C. Heaven, *J. Phys. Chem.* **100**, 18702 (1996).
- ²⁵C. A. Wight, B. S. Ault, and L. Andrews, *J. Chem. Phys.* **65**, 1244 (1976).
- ²⁶A. B. Sannigrahi and S. D. Peyerimhoff, *Int. J. Quantum Chem.* **30**, 413 (1986).
- ²⁷B. R. De and A. B. Sannigrahi, *Int. J. Quantum Chem.* **22**, 435 (1982).
- ²⁸E. Vasini and E. Castro, *J. Mol. Struct.* **22**, 415 (1974).
- ²⁹E. Castro and E. Vasini, *Int. J. Quantum Chem.* **22**, 433 (1982).
- ³⁰D. L. Thomson, *J. Chem. Phys.* **60**, 4557 (1974).
- ³¹J. J. Duggan and R. J. Grice, *J. Chem. Soc. Faraday Trans. 2.* **80**, 809 (1984).
- ³²L. Dalla Riva, S. H. Lin, and H. Eyring, *Anal. Asoc. Quim. Arg.* **59**, 133 (1971).
- ³³G. L. Gutsev, *J. Struct. Chem.* **30**, 733 (1989); G. L. Gutsev, *J. Phys. Chem.* **66**, 1569 (1992); G. L. Gutsev and T. Ziegler, *Can. J. Chem.* **69**, 993 (1991).
- ³⁴Y. T. Lee, R. R. LeBreton, J. D. McDonald, and D. R. Hershbach, *J. Chem. Phys.* **51**, 455 (1969).
- ³⁵K. Yamashita (unpublished).
- ³⁶T. G. Wright and E. P. F. Lee, *Mol. Phys.* **79**, 995 (1993).

- ³⁷J. M. Galbraith, T. J. Van Huis, M. L. Leininger, G. Vacek, and H. F. Schaefer (private communication).
- ³⁸MOLPRO 96, H.-J. Werner and P. J. Knowles, University of Birmingham, U.K. (1996).
- ³⁹T. H. Dunning, Jr., *J. Chem. Phys.* **90**, 1007 (1989).
- ⁴⁰H.-J. Werner and P. J. Knowles, *J. Chem. Phys.* **82**, 5053 (1985); P. J. Knowles and H.-J. Werner, *Chem. Phys. Lett.* **115**, 259 (1985); H.-J. Werner and W. Meyer, *J. Chem. Phys.* **74**, 5794 (1981).
- ⁴¹H.-J. Werner and P. J. Knowles, *J. Chem. Phys.* **89**, 5803 (1988); P. J. Knowles and H.-J. Werner, *Chem. Phys. Lett.* **145**, 514 (1988); H.-J. Werner and P. J. Knowles, *Theor. Chim. Acta* **78**, 175 (1990).
- ⁴²B. O. Roos, Per Linse, Per E. M. Siegbahn, and M. R. A. Blomberg, *Chem. Phys.* **66**, 197 (1982); H.-J. Werner, *Mol. Phys.* **89**, 645 (1996); K. Andersson, Per A. Malmqvist, B. O. Roos, A. J. Sadlej, and K. Wolinski, *J. Phys. Chem.* **94**, 5483 (1990); See also K. Andersson, *Theor. Chim. Acta* **91**, 31 (1995); S. Yamanaka, M. Okumura, K. Yamaguchi, and K. Hirao, *Chem. Phys. Lett.* **225**, 213 (1994).
- ⁴³S. F. Boys and F. Bernardi, *Mol. Phys.* **19**, 553 (1970).
- ⁴⁴S. D. Peyerimhoff and R. J. Buenker, *Chem. Phys.* **57**, 279 (1981).
- ⁴⁵K. P. Huber and G. Herzberg, *Molecular Spectra and Molecular Structure, Constants of Diatomic Molecules, Vol. IV* (Van Nostrand, New York, 1979).
- ⁴⁶M. W. Schmidt, K. K. Baldrige, J. A. Boatz, S. T. Elbert, M. S. Gordon, J. H. Jensen, S. Koseki, N. Matsunaga, K. A. Nguyen, S. J. Su, T. L. Windus, M. Dupuis, and J. A. Montgomery, *J. Comput. Chem.* **14**, 1347 (1993).
- ⁴⁷G. D. Purvis III and R. J. Bartlett, *J. Chem. Phys.* **76**, 1910 (1992).
- ⁴⁸J. Gauss, W. J. Lauderdale, J. F. Stanton, J. D. Watts, and R. J. Bartlett, *Chem. Phys. Lett.* **182**, 207 (1991).
- ⁴⁹J. Gauss, J. F. Stanton, and R. J. Bartlett, *J. Chem. Phys.* **95**, 2623 (1991).
- ⁵⁰See for example J. F. Stanton, J. Gauss, and R. J. Bartlett, *Chem. Phys. Lett.* **195**, 194 (1992); J. Gauss, J. F. Stanton, and R. J. Bartlett, *J. Chem. Phys.* **97**, 7825 (1992).
- ⁵¹R. Trainham, G. D. Fletcher, and D. J. Larson, *J. Phys. B: At. Mol. Phys.* **20**, L777 (1987).
- ⁵²M.-L. Dubernet and J. M. Hutson, *J. Chem. Phys.* **101**, 1939 (1994).